Wall-related Raman scattering in ferroelastic lead phosphate $Pb_3(PO_4)_2$

2001 J. Phys.: Condens. Matter 13 9383

(http://iopscience.iop.org/0953-8984/13/41/323)

INSTITUTE OF PHYSICS PUBLISHING JOURNAL OF PHYSICS: CONDENSED MATTER

J. Phys.: Condens. Matter **13** (2001) 9383–9392 PII: S0953-8984(01)24083-1

Wall-related Raman scattering in ferroelastic lead phosphate $Pb_3(PO_4)_2$

B Mihailova[1,2], U Bismayer[1], A Engelhardt[3] and B Güttler[4]

[1] Mineralogisch-Petrographisches Institut, Universität Hamburg, Grindelallee 48, 20146 Hamburg, Germany
[2] Central Laboratory of Mineralogy and Crystallography, Bulgarian Academy of Sciences, Acad. G Bonchev Street, Building 107, 1113-Sofia, Bulgaria
[3] Institut für Mineralogie, Universität Hannover, Welfengarten 1, 30167 Hannover, Germany
[4] Physikalisch-Technische Bundesanstalt, Bundesallee 100, 38116 Braunschweig, Germany

E-mail: mi0a007@uni-hamburg.de

Received 19 April 2001, in final form 16 August 2001
Published 28 September 2001
Online at stacks.iop.org/JPhysCM/13/9383

Abstract

Micro-Raman spectroscopy is applied to study structural changes in the vicinity of the domain walls in ferroelastic lead phosphate $Pb_3(PO_4)_2$. The Raman spectra measured in untwinned and in heavily twinned regions of monoclinic $Pb_3(PO_4)_2$ are studied and the observed differences are analysed on the basis of calculated vibrational modes of monoclinic structural units with different atomic arrangements. The wall-related Raman signals observed near 537, 65 and 51 cm^{-1} result from static displacements of the Pb_2 atoms along the monoclinic binary axis. PO_4 tetrahedra of rhombohedral geometry can also contribute to the extra Raman scattering near 537 cm^{-1}. The deviations of the Pb_2 atoms from their monoclinic positions couple preferably within the Pb_2–O sheets parallel to the cleavage plane. Rearrangements of the Pb_2 atoms occurring across the domain walls affect the intensity ratios between out-of-plane and in-plane components of $\nu_4(PO_4)$ bending, PO_4 rotational and PO_4 translational modes.

1. Introduction

Lead phosphate is an intensively studied material which undergoes a ferroelastic transformation from a high-temperature rhombohedral to a low-temperature monoclinic phase. The phase transition has been explained in terms of a three-states Potts model including displacive and order–disorder characteristics [1]. Around 560 K, a displacive structural modification involving small shifts of Pb positions from the ternary axis in the three possible directions of the monoclinic binary axis takes place. The local symmetry becomes monoclinic, although the global symmetry is still trigonal. The ferroelastic transition point occurs at 453 K,

where a preferential orientation of the monoclinic binary axis is realized and macroscopic ferroelastic domains appear. Twinning yields typical W and W′ walls in the low-temperature ferroelastic phase stemming from the symmetry elements *m* and *2* of the paraphase. Ferroelastic domains represent energetically equivalent orientation states described by spontaneous strain tensors [2, 3]. However, the domain pattern can also be influenced by some external field or by changing the chemical composition [4, 5]. Domains are separated by domain walls with finite width [6–9]. The walls were described as plane walls with an orientation predictable from the symmetry of the system and the ferroelastic strain [2]. The re-orientation of the order parameter between neighbouring domains is considered on an atomic level as a sequence of dislocations such that the lattices on either side of the wall correspond to each other by a simple rotation referred to as a coordinate system linked to the wall [10]. Perpendicularly running walls of different types are classified as W and W′. Although some theoretical studies on mesoscopic structures on the surface structure of domain walls and simulations of mesocopic patterns are available [8, 9, 11, 12], experimental observations of the domain structure morphology in real crystals are still rare [13, 14]. The size and shape of the domain microstructure have been observed on different length scales by optical microscopy, transmission electron microscopy and atomic force microscopy [15–18]. However, the atomic-scale picture of structural modification near the domain walls is still not clear and needs further investigations.

Raman spectroscopy is a method widely applied for studying the local structure in crystals with defects and partially disordered systems. Spatial regions, ∼10 Å in size, can be detected by Raman scattering measurement. Recently, wall-related changes in the spectrum profile of the Raman-active hard modes in lead phosphate have been reported [18]. The aim of the present paper is to clarify the origin of the wall-related Raman signals observed below 700 cm^{-1} in the spectrum of the ferroelastic phase of $Pb_3(PO_4)_2$. For this reason, the differences between the spectra of samples without and with a high concentration of domain walls are analysed on the basis of calculated vibrational modes of monoclinic structural species.

2. Experimental

Raman spectrometric measurements were performed at room temperature using a triple monochromator system Jobin-Yvon T64 000 equipped with a liquid-N_2-cooled CCD camera. The spectra were collected in a back-scattering geometry using the 514.5 nm line of an Ar^+ ion laser and keeping the output laser power at 100 mW. The exciting laser beam was focused through an Olympus BH2 20× microscope objective on the sample surface which was parallel to the cleavage plane. The diameter of the laser spot on the sample surface was approximately 6 μm. The spectral resolution was about 2 cm^{-1}. Unpolarized Raman spectra from untwinned and heavily twinned regions of the same crystal were recorded. In the latter case about 80 domain walls were in the focus of the beam as estimated from the twin spacing measured by electron microscopy [7]. The orientation of the sample and the experimental parameters remained unchanged during the slight shift of the sample to adjust the laser spot to untwinned or twinned regions.

3. Results and discussion

Figure 1 presents the Raman spectra taken from areas without domain walls, S_0, and with high density of W domain walls, S_W. Several differences between the spectra of S_0 and S_W are visible:

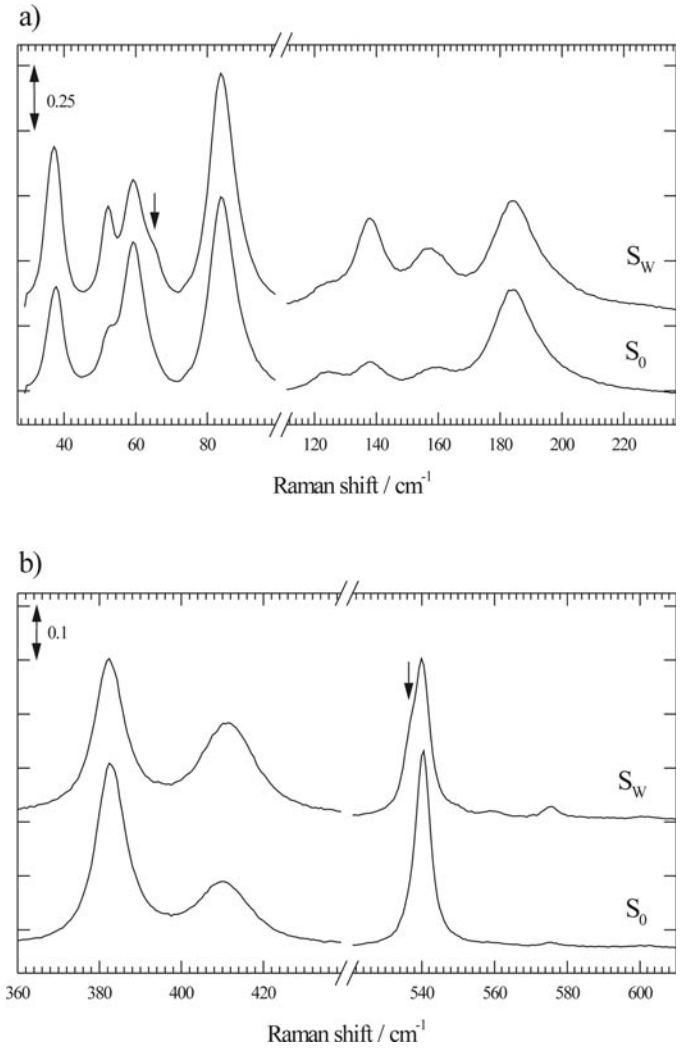

Figure 1. Raman spectra measured at room temperature in untwinned (S_0) and heavily twinned (S_W) areas of $Pb_3(PO_4)_2$. The arrows mark the extra Raman signals near 537 and 65 cm^{-1} observed in the spectrum of S_W.

(i) A low-frequency shoulder of the peak at 541 cm^{-1} appears in the spectrum of S_W.
(ii) The intensity ratios $\frac{I(\omega=138)}{I(\omega=123)}$, $\frac{I(\omega=159)}{I(\omega=184)}$ and $\frac{I(\omega=410)}{I(\omega=382)}$ are larger in the spectrum of S_W than those of S_0.
(iii) An extra peak at about 65 cm^{-1} exists in the spectrum of S_W and the intensity ratio $\frac{I(\omega=52)}{I(\omega=62)}$ is larger in the spectrum of S_W than that of S_0.

To clarify the origin of the observed differences between the Raman spectra of untwinned and heavily twinned areas, first we calculated the vibrational modes of $Pb_3(PO_4)_2$ in a force constant approximation. In this approach a relatively small structural unit, representative of crystal symmetry and atomic bonding, is considered. The frequencies and the atom vector displacements of the normal modes of the structural unit were obtained through diagonalization of its dynamical matrix. The dynamical matrix was calculated in Cartesian

coordinates, without any symmetry constraints in the computing procedure, as a sum of the terms corresponding to two-particle and three-particle interactions [19, 20]. The polarizability tensor and, consequently, the Raman intensities of the modes were calculated from the atomic displacements and bond polarizabilities [21, 22].

The structure of the $Pb_3(PO_4)_2$ paraphase has $R\bar{3}m$ space group symmetry with two types of Pb occupying 3a and 6c Wyckoff positions, one P in 6c Wyckoff position and two types of O in 6c and 18h Wyckoff positions. The symmetry of the ferrophase is $C2/c$ with one Pb in 4e Wyckoff position and the remaining Pb, P and O atoms in 8f Wyckoff position [23]. According to the site group analysis, the atoms in the rhombohedral and monoclinic phases give rise to normal modes of the following symmetry [24]:

$R\bar{3}m$:	$C2/c$:
Pb_1 (3a): $A_{2u} + E_u$	Pb_1 (4e): $A_g + A_u + 2B_g + 2B_u$
Pb_2 (6c): $A_{1g} + A_{2u} + E_g + E_u$	Pb_2 (8f): $3A_g + 3A_u + 3B_g + 3B_u$
P (6c): $A_{1g} + A_{2u} + E_g + E_u$	P (8f): $3A_g + 3A_u + 3B_g + 3B_u$
O_t (6c): $A_{1g} + A_{2u} + E_g + E_u$	O_t (8f): $3A_g + 3A_u + 3B_g + 3B_u$
O_p (18h): $2A_{1g} + A_{1u} + A_{2g} + 2A_{2u} + 3E_g + 3E_u$	$O_p^{(1)}$ (8f): $3A_g + 3A_u + 3B_g + 3B_u$
	$O_p^{(2)}$ (8f): $3A_g + 3A_u + 3B_g + 3B_u$
	$O_p^{(3)}$ (8f): $3A_g + 3A_u + 3B_g + 3B_u$.

Thus $5A_{1g} + 6E_g$ modes are Raman-active in the paraphase and $19A_g + 20B_g$ modes are Raman-active in the ferrophase of $Pb_3(PO_4)_2$.

The structure of $Pb_3(PO_4)_2$ can be considered as being built of layers of PO_4 tetrahedra and PbO_n polyhedra, parallel to the cleavage plane [25]. In the high-temperature phase ($R\bar{3}m$) the layers are perpendicular to the hexagonal c-axis and the layer repeating unit is composed of two PO_4 tetrahedra linked to two Pb_2 atoms and one Pb_1 atom (figure 2(a)). In the low-temperature phase ($C2/c$) the layers are perpendicular to the pseudo-threefold axis which makes an angle of 18° with the monoclinic a-axis. The repeating unit is twice as big as the corresponding one in the rhombohedral phase (figure 2(b)). Hence, by imposing periodic boundary conditions on the clusters shown in figures 2(a) and (b) we modelled the normal modes of rhombohedral and monoclinic $Pb_3(PO_4)_2$. The topic oxygens, O_t, positioned at the tetrahedral vertices, and the plane oxygens, O_p, forming the tetrahedral bases, have quite different atomic surroundings. Each O_t atom is strongly bonded to one Pb_2 atom and interacts weakly with three Pb_1 atoms, whereas each O_p atom forms weaker bonds with one Pb_1 and two Pb_2 atoms in the layer and, in addition, interacts weakly with one Pb_2 atom from the neighbouring layer. The surroundings of the two types of lead atoms are described as follows: Pb_1 forms weak bonds with six O_p atoms and interacts weakly with six O_t atoms, while Pb_2 forms a strong bond with one O_t atom and weaker bonds with six O_p within the layer. Also Pb_2 interacts weakly with three O_p atoms in the next layer. On the basis of this coordination spheres we specified the set of force constants used in the calculations of the vibrational modes. The non-equivalence of the O_t and O_p atoms is defined either by using different force constant values for the O_p–P–O_t and O_p–P–O_p bond bending interactions or including O_t–O_p interactions in the potential. The values of the force constants used in the two cases are given in table 1. Table 2 contains the calculated frequencies of the Raman-active modes of the rhombohedral and the monoclinic structural units, the mode symmetry and the type of vibrations. The results obtained are in a good accord with the atom-type participation in the normal modes, as predicted by the site group analysis. For comparison, the frequencies of the peaks observed at room temperature in

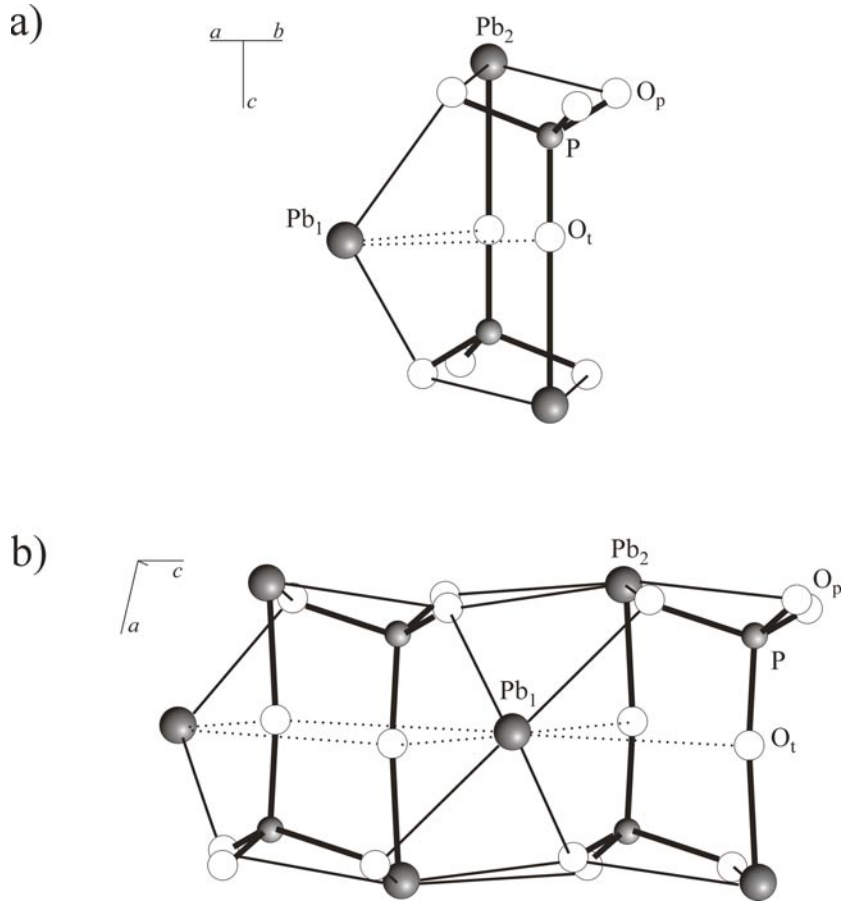

Figure 2. Rhombohedral (a) and monoclinic (b) structural species used for modelling the Raman-active modes in a $Pb_3(PO_4)_2$ single crystal. Modification of the Pb-configuration in the monoclinic species can be realized by mutual shifts of Pb_2 atoms within one Pb_2–O_p sheet or in adjacent sheets.

the Raman spectrum of a $Pb_3(PO_4)_2$ sample without domain walls are included in table 2. We find that the calculated frequencies of the P–O stretching modes fit much better the observed peak positions when O_t–O_p interactions are taken into account. Hence, the corresponding set of force constants was used to model the wall-related Raman signals. The choice of the force constant set affects the calculated frequencies of the internal tetrahedral modes; however, it has no impact on peak identification and mode dependence on structural changes in the clusters considered.

Generally the Raman scattering from A_g modes is much stronger than that from B_g modes, and hence we consider that the A_g modes contribute mainly to the unpolarized Raman spectrum of $Pb_3(PO_4)_2$. The peaks observed were finally assigned as shown in table 3. Some comments concerning PO_4 bending modes should be made. The Pb sublattice substantially influences the eigenfrequencies of the PO_4 tetrahedra. Particularly, the Pb_2–O_t–P interactions affect the frequency difference between the two A_g modes at 541 and 575 cm^{-1}, which corresponds to ν_2 of a free PO_4 group. Besides, these modes differ from each other in the contribution of the O_t, O_p and P atoms. This results in a substantially larger *cc*-component of the polarizability

Table 1. Force constants used in the calculations.

	Force constant value (N m^{-1})	
Type of interaction	Set 1	Set 2
P–O stretching	740	530
O_p–P–O_p bending	30	30
O_p–P–O_t bending	80	30
O_p–O_t interaction		142
Pb_1–O_p stretching	15	15
O_p–Pb_1–O_p bending	0.1	0.1
Pb_1–O_p–P bending	0.1	0.1
Pb_1–O_t interaction	0.1	0.1
Pb_2–O_t stretching	40	40
Intralayer Pb_2–O_p stretching	7	7
Interlayer Pb_2–O_p interactions	3	3
O_p–Pb_2–O_p bending	1.5	1.5
O_p–Pb_2–O_t bending	4	4
Pb_2–O_p–P bending	6	6
Pb_2–O_t–P bending	12	12
Pb–O_p–Pb bending	0.1	0.1

tensor for lower frequency mode, which is in excellent agreement with our experimentally observed Raman profile. Benoit and Chapelle have reported Raman peaks at 542, 552 and 602 cm^{-1} as originating from $\nu_4(PO_4)$ [26]. Our observation yields very weak signals around 552 and 602 cm^{-1}. The out-of-plane component of $\nu_4(PO_4)$ might give rise to the weak observable peak at 575 cm^{-1} (see figure 1), but there is no reason to assign both the intense peak at 541 cm^{-1} and the very weak peak at 559 cm^{-1} to in-plane $\nu_4(PO_4)$ vibrations, because the two in-plane components of $\nu_4(PO_4)$ must have the same intensity in the experimental geometry used. Thus our experimental findings suggest that the peaks generated by O–P–O bending modes should be re-assigned as given in table 2.

It has been shown by Novak *et al* that in the vicinity of the W walls, a violation of the local symmetry of the structure occurs [8, 9] and diffuse x-ray scattering data confirm these findings [17, 18]. The width of a domain wall is finite and the order parameter on either side of the wall has a different sign. The variation from one domain to its neighbour can be approximated by $Q^2 \propto \tanh(r/w)$, where r is a space coordinate perpendicular to the wall and w is the wall thickness (see figure 3). Inside the wall a gradient of static displacements of Pb atoms along the b-axis occurs with vanishing displacements corresponding to the high-temperature phase in its centre. The 'soft mode' near 38 cm^{-1} shifts slightly towards lower energy for $Pb_3(PO_4)_2$ with high domain wall density and chemical changes [27]. The observed frequency shift and the extra Raman signals suggest that intermediate structural species of different monoclinic deformations occur. Thus we calculated the vibrational modes of different 'pseudo'-monoclinic units, namely (i) when one or both Pb_1 atoms are shifted from their monoclinic to their rhombohedral positions; (ii) when one, two, three or all four Pb_2 atoms are displaced along the b-axis and (iii) when the geometry of PO_4 tetrahedra corresponds to that in the paraphase.

Our calculations show that the shift of the Pb_1 atoms along the b-axis affects only the 'soft' mode near 38 cm^{-1}, lowering its frequency slightly. The influence of the Pb_2 arrangement on the lattice dynamics is stronger and more complex. In addition to the softening of the

Table 2. Calculated frequencies, symmetry and type of vibration of the Raman-active modes in paraelastic ($R\bar{3}m$) and ferroelastic ($C2/c$) phases of $Pb_3(PO_4)_2$.

ω_{exp} (cm^{-1}) at room temperature T	ω_{calc} (cm^{-1}) Rhombohedral species		ω_{calc} (cm^{-1}) Monoclinic species		Type of vibration[a]
	Set 1	Set 2	Set 1	Set 2	
1002	1196	1076 A_{1g}	1209	1075 A_g	$\nu_3(PO_4)$, op P–O_t stretching
			1210	1075 B_g	$\nu_3(PO_4)$, op P–O_t stretching
989	1193	1035 E_g	1200	1042 A_g	$\nu_3(PO_4)$, ip P–O_p stretching
			1201	1043 B_g	$\nu_3(PO_4)$, ip P–O_p stretching
955			1178	1024 A_g	$\nu_3(PO_4)$, ip P–O_p stretching
			1178	1025 B_g	$\nu_3(PO_4)$, ip P–O_p stretching
932	903	923 A_{1g}	903	929 A_g	$\nu_1(PO_4)$, sym P–O stretching
			903	929 B_g	$\nu_1(PO_4)$, sym P–O stretching
575 w			581	579 A_g	$\nu 2(PO_4)$, sym O–P–O bending
595 vw			579	577 B_g	$\nu 2(PO_4)$, sym O–P–O bending
541	540	539 E_g	542	541 A_g	$\nu 2(PO_4)$, sym O–P–O bending
559 vw			538	537 B_g	$\nu 2(PO_4)$, sym O–P–O bending
410	477	439 A_{1g}	476	437 A_g	$\nu_4(PO_4)$, op O_p–P–O_t bending
			474	436 B_g	$\nu_4(PO_4)$, op O_p–P–O_t bending
382	385	382 E_g	385	382 A_g	$\nu_4(PO_4)$, ip O_p–P–O_p bending
			386	383 B_g	$\nu_4(PO_4)$, ip O_p–P–O_p bending
			381	379 A_g	$\nu_4(PO_4)$, ip O_p–P–O_p bending
			381	379 B_g	$\nu_4(PO_4)$, ip O_p–P–O_p bending
184			207	207 A_g	ip O_p twisting, i.e., ip PO_4 rotation
			204	204 B_g	ip O_p twisting, i.e., ip PO_4 rotation
			194	194 A_g	ip+op PO_4 rotation
			210	210 B_g	op PO_4 rotation
159	158	158 E_g	152	152 A_g	op PO_4 rotation
			176	176 B_g	op PO_4 rotation
138	142	142 A_{1g}	141	141 A_g	op PO_4 translation
			138	138 B_g	op PO_4 translation
123	115	115 E_g	119	119 A_g	ip PO_4 translation
			128	128 B_g	ip PO_4 translation
			113	113 A_g	ip PO_4 translation
			112	112 B_g	ip PO_4 translation
84	83	83 A_{1g}	83	83 A_g	op Pb_2 vibration and weak op PO_4 translation
			78	78 B_g	op Pb_2 vibration and weak op PO_4 translation
62			60	60 A_g	Pb_2 and weak PO_4 translation || b
			52	52 B_g	Pb_2 and weak PO_4 tanslation || b op Pb_1 vibration
52			51	51 A_g	Pb_2 and weak PO_4 translation || c
			62	62 B_g	Pb_2 and weak PO_4 translation || c op Pb_1 vibration
	52	52 E_g			ip Pb_2 vibration and weak ip PO_4 translation
38			37	37 A_g	Pb_1 vibration and weak PO_4 translation || b
			37	37 B_g	Pb_1 and Pb_2 vibrations $\perp b$
			34	34 B_g	Pb_1 and Pb_2 vibrations $\perp b$

[a] op, out-of-plane; ip, in-plane; O_t, topic oxygen; O_p, plane oxygen.

Table 3. Assignment of the peaks observed at room temperature in the Raman spectrum of a $Pb_3(PO_4)_2$ single crystal.

ω_{exp} (cm^{-1})	ω_{calc} (cm^{-1})	Symmetry	Type of vibration[a]
1002	1075	A_g	$\nu_3(PO_4)$, op P–O_t stretching
989	1042	A_g	$\nu_3(PO_4)$, ip P–O_p stretching
955	1024	A_g	$\nu_3(PO_4)$, ip P–O_p stretching
932	929	A_g	$\nu_1(PO_4)$, sym P–O stretching
575	579	A_g	$\nu_2(PO_4)$, sym O–P–O bending
541	541	A_g	$\nu_2(PO_4)$, sym O–P–O bending
410	437	A_g	$\nu_4(PO_4)$, op O_p–P–O_t bending
382	382	A_g	$\nu_4(PO_4)$, ip O_p–P–O_p bending
	379	A_g	$\nu_4(PO_4)$, ip O_p–P–O_p bending
184	207	A_g	ip O_p twisting, i.e., ip PO_4 rotation
	194	A_g	ip+op PO_4 rotation
159	152	A_g	op PO_4 rotation
138	141	A_g	op PO_4 translation
123	119	A_g	ip PO_4 translation
	113	A_g	ip PO_4 translation
84	83	A_g	op Pb_2 vibrations and weak op PO_4 translation
62	60	A_g	ip Pb_2 vibrations and weak ip PO_4 translation (along *b*)
52	51	A_g	ip Pb_2 vibrations and weak ip PO_4 translation (along *c*)
38	37	A_g	ip Pb_1 vibration (along *b*)

[a] op, out-of-plane; ip, in-plane; O_t, topic oxygen; O_p, plane oxygen.

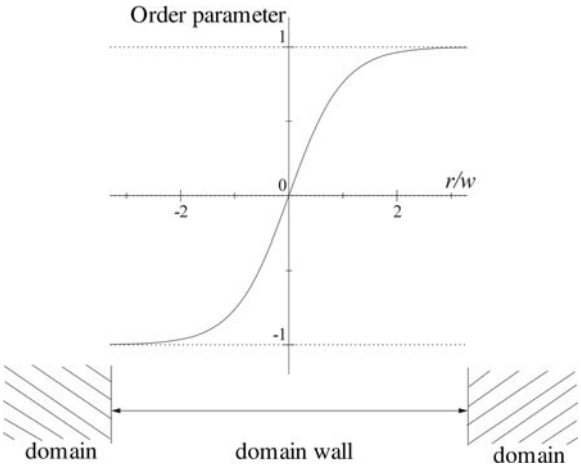

Figure 3. Order parameter profile across a domain wall.

lowest frequency A_g mode, the deviation of the Pb_2 atoms from monoclinic to rhombohedral positions decreases the frequency of the $\nu_2(PO_4)$ vibration. Moreover, the spectral range 40–70 cm^{-1} is modified in a different way depending on the Pb_2 configuration. When the

Pb_2 atoms of one Pb_2–O_p sheet are in a rhombohedral position (see figure 2(b)), the B_u mode with a calculated frequency 65 cm^{-1}, consisting of out-of-plane Pb_1 and Pb_2 motions, becomes Raman-active. This most probably generates the extra Raman signal observed in the spectrum of heavily twinned $Pb_3(PO_4)_2$. Besides, in such a Pb_2 configuration the two A_g modes involving in-plane Pb_2 vibrations appear close in frequency, i.e. at 52 and 50 cm^{-1} instead of 60 and 51 cm^{-1}. This fits well to the observed difference in the intensity ratio $\frac{I(\omega=52)}{I(\omega=62)}$ between untwinned and twinned samples. On the other hand, configurations with Pb_2 atoms in rhombohedral position which are placed on opposite sides of the layer do not generate vibrations fitting the spectral profile observed in the range 45–70 cm^{-1}. This suggests that there is strong correlation between Pb_2 displacements along the Pb–Pb_4 layer rather than across the layer. A change in the geometry of the PO_4 tetrahedra from 'monoclinic' to 'rhombohedral' also causes a frequency shift of the $\nu_2(PO_4)$ to lower energy. Therefore, the appearance of the low-frequency shoulder of the peak at 541 cm^{-1} is caused by both the Pb rearrangement and the existence of PO_4 species of rhombohedral symmetry.

Summarizing the calculated dependence of the modes on different structural changes, one can assume that across the domain walls 'rhombohedral' PO_4 tetrahedral species are formed and specific Pb rearrangements occur according to the profile of the order parameter. Deviations of the Pb_2 atoms from their monoclinic positions correlate preferably within the Pb_2–O_p sheets rather than perpendicular to the sheets, which disrupts the inter-layer periodicity. Spatial areas where such structural changes exist contribute to the Raman scattering at about 537, 65 and 51 cm^{-1}.

It has been shown that in $Pb_3(PO_4)_2$, the Pb_2 atoms possess lone-pair electrons [25]. The lone pairs are perpendicular to the layers in the rhombohedral state and are slightly tilted in the monoclinic state. Therefore, one can expect that the orientations of the lone pairs of the Pb_2 atoms shifted from their monoclinic positions are changed, which should lead to the formation of local anisotropic polarization fields. Such local fields affect the electron density of states in the lattice, thus changing the bond polarizabilities. Especially the Pb_2–O_p–P linkages due to the local symmetry of the O_p positions are influenced. Consequently, the intensity of those modes which involve out-of-plane atomic displacements is expected to increase with increasing domain wall concentration, while the intensity of the modes involving in-plane vibrations should decrease. In fact, such changes in the intensity ratios between the out-of-plane and in-plane components are observed for the PO_4 translational mode (the peaks near 138 and 123 cm^{-1}), the PO_4 rotational mode (the peaks near 159 and 184 cm^{-1}) and for the asymmetrical bending mode $\nu_4(PO_4)$ (the peaks near 410 and 382 cm^{-1}).

4. Conclusions

The phonons in the spatial areas in the vicinity of the domain walls differ from those in the domain bulk and their contribution to the Raman spectrum is experimentally observed in heavily twinned samples. The wall-related Raman signal observed near 537 cm^{-1} is due to the existence of rhombohedral PO_4 species as well as the Pb re-arrangement occurring near the domain walls, whereas those observed at 65 and 51 cm^{-1} result mainly from static displacements of the Pb_2 atoms along the monoclinic binary axis. The deviations of the Pb_2 atoms from their monoclinic positions correlate preferably within the Pb_2–O_p sheets. In addition, the existence of domain walls affects the intensity ratios between in-plane and out-of-plane components of $\nu_4(PO_4)$ bending and PO_4 rotation and translation modes due to the re-orientation of the lone pairs of the shifted Pb_2 atoms.

Acknowledgments

BM is indebted to the Alexander von Humboldt Foundation for a scholarship. UB acknowledges financial support from the Deutsche Forschungsgemeinschaft.

References

[1] Salje E and Devarajan V 1981 *J. Phys. C: Solid State Phys.* **14** L1029
[2] Bismayer U and Salje E 1981 *Acta Crystallogr.* A **37** 45
[3] Bismayer U, Hensler J, Salje E and Güttler B 1994 *Phase Transitions* **48** 149
[4] Auzu K 1970 *J. Phys. Soc. Japan* **28** 706
[5] Kleman M and Schlenker M 1972 *J. Appl. Phys.* **43** 3184
[6] Wruck B, Salje E K H, Zhang M, Abraham T and Bismayer U 1994 *Phase Transitions* **48** 135
[7] Hayward S A, Chrosch J, Salje E K H and Carpenter M 1996 *Eur. J. Mineral.* **8** 1301
[8] Novak J and Salje E K H 1998 *J. Phys.: Condens. Matter* **10** L359
[9] Novak J and Salje E K H 1998 *Eur. Phys. J.* B **4** 279
[10] Torres J, Rouceau C and Ayroles R 1982 *Phys. Status Solidi a* **70** 193
[11] Salje E K H and Ishibashi Y 1996 *J. Phys.: Condens. Matter* **8** 8477
[12] Salje E K H, Bismayer U, Hayward S and Novak J 2000 *Mineral. Mag.* **64** 201
[13] Bosbach D, Putnis A, Bismayer U and Güttler B 1997 *J. Phys.: Condens. Matter* **9** 8397
[14] Bueble S, Knorr K, Brecht E and Schmahl W 1998 *Surf. Sci.* **400** 345
[15] Bismayer U, Hensler J, Salje E and Güttler B 1994 *Phase Transitions* **48** 149
[16] Salje E K H, Buckley A, van Tendeloo G, Ishibashi Y and Nord G L 1998 *Am. Mineral.* **83** 811
[17] Bismayer U, Mathes D, Bosbach D, Putnis A, van Tendeloo G, Novak J and Salje E K H 2000 *Mineral. Mag.* **64** 233
[18] Bismayer U, Mathes D, Aroyo M, Bosbach D, Putnis A, van Tendeloo G and Güttler B 2000 *Phase Transitions* **71** 243
[19] Furukawa T, Fox K E and White W B 1981 *J. Chem. Phys.* **75** 3226
[20] Mihailova B, Zotov N, Marinov M, Nikolov J and Konstantinov L 1994 *J. Non-Cryst. Solids* **168** 265
[21] Lippincott E and Stutman J 1964 *J. Phys. Chem.* **68** 2926
[22] Bell R J 1976 *Meth. Comput. Phys.* **15** 215
[23] Guimaraes D M C 1979 *Acta Crystallogr.* A **35** 108
[24] Rousseau D L, Bauman R P and Porto S P S 1981 *J. Raman Spectrosc.* **10** 253
[25] Kiat J M, Garnier P and Pinot M 1991 *J. Solid State Chem.* **91** 339
[26] Benoit J P and Chapelle J P 1974 *Solid State Commun.* **15** 531
[27] Salje E, Devarajan V, Bismayer U and Guimaraes D M C 1983 *J. Phys. C: Solid State Phys.* **16** 5233